# Exploring the super-relaxed state of myosin in myofibrils from fast-twitch, slow-twitch, and cardiac muscle

**Jonathan Walklate**[1], **Kerry Kao**[2], **Michael Regnier**[2], and **Michael A. Geeves**[1],*

*From the [1]School of Biosciences, Division of Natural Sciences, University of Kent, Canterbury, UK; [2]Department of Bioengineering, University of Washington, Seattle, Washington, USA*

Edited by Enrique De La Cruz

**Muscle myosin heads, in the absence of actin, have been shown to exist in two states, the relaxed (turnover ~0.05 s⁻¹) and super-relaxed states (SRX, 0.005 s⁻¹) using a simple fluorescent ATP chase assay (Hooijman, P. et al (2011) Biophys. J. 100, 1969–1976). Studies have normally used purified proteins, myosin filaments, or muscle fibers. Here we use muscle myofibrils, which retain most of the ancillary proteins and 3-D architecture of muscle and can be used with rapid mixing methods. Recording timescales from 0.1 to 1000 s provides a precise measure of the two populations of myosin heads present in relaxed myofibrils. We demonstrate that the population of SRX states is formed from rigor cross bridges within 0.2 s of relaxing with fluorescently labeled ATP, and the population of SRX states is relatively constant over the temperature range of 5 °C–30 °C. The SRX population is enhanced in the presence of mavacamten and reduced in the presence of deoxy-ATP. Compared with myofibrils from fast-twitch muscle, slow-twitch muscle, and cardiac muscles, myofibrils require a tenfold lower concentration of mavacamten to be effective, and mavacamten induced a larger increase in the population of the SRX state. Mavacamten is less effective, however, at stabilizing the SRX state at physiological temperatures than at 5 °C. These assays require small quantities of myofibrils, making them suitable for studies of model organism muscles, human biopsies, or human-derived iPSCs.**

Muscle ATPase activity is traditionally considered to be activated by an increase in cellular calcium, which activates the thin filament (actin, Tpm, and Tn) and allows access of the myosin motors to their binding site on actin. In the last 10 years, attention has shifted to thick filament regulation and mechanisms that may control the number of myosin heads available to interact with actin (1–4). This could provide a mechanism to match the number of active heads to the power requirements of the muscle and thus provide a way to increase the efficiency of the working muscle (5). This off-state of the thick filament also provides a very low ATPase turnover rate and has been proposed to be utilized in hibernating states, the super-relaxed or SRX state (5, 6).

Several descriptions of the thick filament regulation have been explored both structurally and functionally. One explored structurally, in muscle fibers and in isolated thick filaments, is the order–disorder transition of the thick filaments revealed by electron microscopy (7–10), X-ray crystallography (11–14), and fluorescence polarization probes on the myosin motor (15). Several factors have been shown to perturb the balance between the ordered and disordered myosin states within the thick filament including temperature (11, 12), the conformation of the myosin's motor and several small-molecule drugs (16, 17).

Work on isolated skinned muscle fibers, myofibrils, myosin thick filaments, heavy meromyosin (HMM), and myosin has revealed the presence of two populations of "relaxed" myosin heads (16, 18–20). Those with the typical ATPase turnover rate of a single isolated motor domain (0.05 s-1), and a second population with a much slower turnover rate (~0.005 s-1) the SRX population. The two populations appear to be in a quasi-equilibrium, which can be perturbed by temperature, ionic strength, small-molecule drugs, and phosphorylation of myosin light chains and myosin-binding protein C (15, 21–23).

The low ATPase activity state has also been associated with an off-state of myosin in which the two heads interact to generate a form of the myosin head (interacting head motif, IHM) equivalent to the 10S/6S transition of smooth muscle myosin (24, 25). Such structures have now been observed by negative stain EM for many two headed myosin, both muscle and nonmuscle (26). The interacting head motif has also been observed in ordered thick filaments consistent with the low ATPase form of myosin being present in the off-state of the filament (14, 27).

The SRX state of myosin in muscle is defined as a form of myosin that has a turnover rate for ATP much slower (up to ten times slower) than seen in the isolated single motor domain of myosin, subfragment 1. It has been most easily monitored using single turnover/chase methods in which a fluorescently labeled ATP is allowed to interact with myosin and come to equilibrium, then is chased off by an excess of unlabeled ATP. Here we use this approach to study myofibrils (small fragments of muscle tissue containing a dozen or so sarcomeres in series). More than 10 years ago, it was shown that the fluorescent ATP analogue 2′/3′-O-(N-Methyl-anthraniloyl)-adenosine-5′-triphosphate (mant-ATP) could be

* For correspondence: Michael A. Geeves, m.a.geeves@kent.ac.uk.

added to rigor myofibrils to measure the rates of relaxation and ATP turnover (19, 28).

Recently, Nag and colleagues (18) demonstrated that this approach was convenient to use with synthetic thick filament. Here we show that it can also be used with myofibrils, which can be made from a variety of muscle tissue samples (cardiac and skeletal) from human as well as model systems and from patient-derived stem cells. The advantage of myofibrils over synthetic thick filaments is the presence of other regulatory elements in the thick filament and the sarcomere such as myosin-binding protein C (MyBP-C), which is thought to have a role in regulating the availability of myosin heads (21). This approach allows a more detailed study of thick filament regulatory systems and may find wide use in the study of skeletal and cardiac myopathies and in defining the mechanism of drug action.

One major question of current interest is if the different types of off states, the SRX and the IHM of myosin, and the ordered/disorder state of myosin thick filaments, are exactly the same or are there populations of the SRX and IHM, which are not ordered on the thick filament backbone. Here we use relaxed myofibrils to investigate if the data are compatible with one or more populations of off-state myosins and demonstrate that there must be more than one population slowly turning over myosin heads.

## Results

### Bovine masseter myofibrils in the stopped flow

To investigate if myofibrils could be used in the stopped flow as a method of probing the population of IHM/SRX myosin, bovine masseter (BM) myofibrils in rigor were pre-incubated with mant-ATP for 1 minute to relax the myofibrils and load each myosin head with M.ADP.$P_i$, before rapidly mixing in the stopped flow with unlabeled "dark" ATP (Fig. 1A). The fluorescence transients were best described by a double exponential as the mant-ATP is displaced from the myofibrils. The two phases represent two populations of myosin heads, those turning over at the steady-state rate consistent with that expected of single isolated head ($\sim$0.027 s$^{-1}$) and a second population turning over approximately tenfold slower ($\sim$0.0036 s$^{-1}$, Table S1) at 20 °C.

The slow and fast phases have previously been associated with the super-relaxed state (SRX; slow component) and disordered relaxed state (DRX; faster component). Fitting the two components accurately requires data collection over the two timescales (half times of $\sim > 25$ and 250 s). The current generation of stopped flow equipment can capture the early events well within in the first 0.1 s after mixing (sufficient to capture events at <1 s$^{-1}$, or half-times of >0.69 s, much faster than the events described here), and the signal is sufficiently stable to define an accurate end point after 1000 s, as required to define the slow phase. We will return to this issue in the discussion.

The fluorescence amplitudes of the two phases indicated the population of the two states of myosin. The measured amplitudes were variable in these tissue derived samples; at 20 °C,

the observed amplitude of the fast phase was a decrease of between 2.6 and 13.5% with an average amplitude of 7.4 ± 0.8%, while the amplitude of the slow phase ranged from 1.6 to 4.4% with an average amplitude of 2.3 ± 0.2% (n = 16). The variability is a result of heterogeneity in the myofibril preparation (heterogeneous size of myofibrils and variability in the degree of aggregation) resulting in changes in both fluorescent signal and the large scattering background. For each measurement assay, the transient was collected more than ten times to generate a well-defined average (Fig. 1B). The average relative population of the two components (proportional to the fast and slow phase amplitudes) was calculated as 74.3% for the fast component and 25.7% for the slow component (SRX) at 20 °C (Fig. 1B).

An important question that has not been addressed to date is how quickly the SRX state is formed on mixing rigor cross-bridges with ATP. In rigor almost all myosin heads are bound to actin and thus cannot form the IHD, an ordered thick filament and by implication the SRX state. The double mixing capabilities of the stopped flow were used to address how quickly the SRX state forms. Firstly, the second-order rate constant of mant-ATP binding to myosin was measured (from the approximately twofold increase in mant fluorescence on binding to myosin (29)) (Fig. 1C) to define how quickly the mant-ATP binds to and relaxes the myofibrils. The data show that the observed rate constant, $k_{obs}$, is linear over the range (1–5 μM) with a second-order rate constant of 3.2 ± 0.03 μM$^{-1}$ s$^{-1}$. The data are compatible with earlier reports of ATP and mant-ATP binding to isolated myosin fragments (29) and myofibrils (28). The high background fluorescence from free mant-nucleotides limits the maximum mant-ATP concentration used to 5 μM when using 50 nM myosin heads in myofibrils. Increasing the myofibril concentration increases the scattering background and therefore reduces % signal change observed. The mant-ATP (5 μM) and myofibril (50 nM myosin heads) concentrations were optimal for the double mixing experiment allowing reasonably fast mant-ATP binding and fluorescence signal change.

In the double mixing study, 5 μM mant-ATP (concentration after the first mixing) was used. This allowed the myofibrils to be mixed with 5 μM mant-ATP for a set time (the age time) before they were mixed with unlabeled ATP (Fig. 1D). There was no significant difference in the observed amplitudes between a 60 s age time and 0.2 s age time suggesting that the myosin enters the SRX within 200 ms and is essentially limited by the rate of mant-ATP binding under these conditions (3.2 μM$^{-1}$ s$^{-1}$ × 5 s$^{-1}$ = 16 s$^{-1}$, $t_{1/2}$ = 46 ms). This leaves an intriguing question of how the SRX is formed within 200 ms but exits from the SRX in more than 100 s. Shorter age times were limited because of the rate of mant-ATP binding at the low concentrations used here. Longer age times were limited by the turnover of mant-ATP and buildup of mant-ADP.

### Mavacamten effects on myofibrils

Mavacamten, a drug developed to treat hypercontractility in hypertrophic cardiomyopathy (HCM), has been shown to
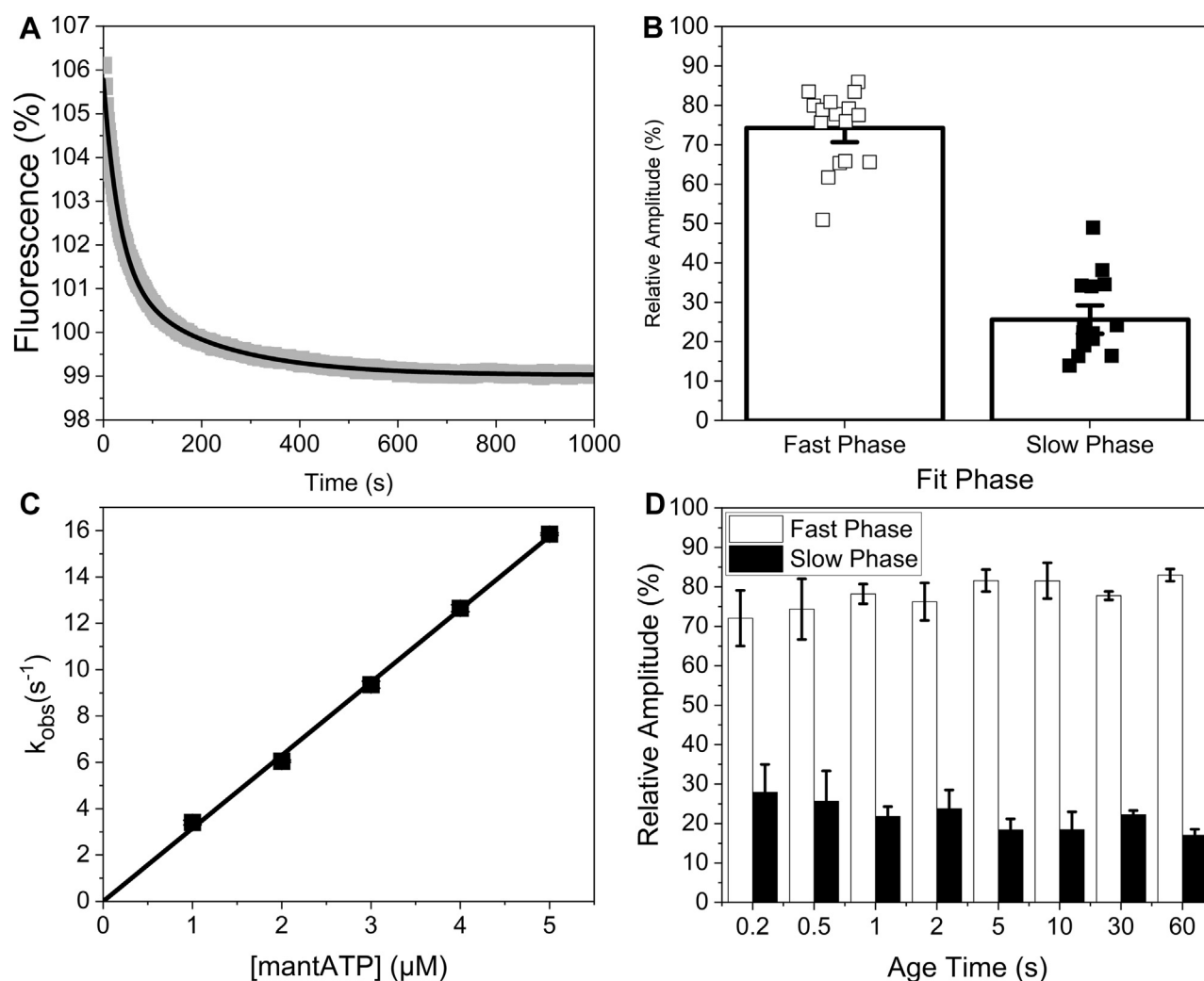
**Figure 1. MantATP association with bovine masseter myofibrils.** *A,* an example transient of 100/50 nM bovine masseter myofibrils incubate with 10/5 μM mant-ATP for 1 min then rapidly mixed with 250/125 μM MgATP in the stopped flow. This was best described by a double exponential, resulting in a $k_{obs}$ = 0.027 s$^{-1}$ and 0.0038 s$^{-1}$ for the fast and slow phase respectively and an amplitude of 5.6% and 1.6% for the fast and slow phase, respectively. *B,* relative amplitudes of the fast (DRX, *open squares*) and slow (SRX, *closed squares*) phases of mant-ATP displacement from bovine masseter myofibrils at 20 °C. *C,* plot of the observed rate constant of mant-ATP binding to bovine masseter myofibrils using single mixing. The second-order on-rate constant derived from the slope ($K_1 k_{+2}$) = 3.2 ± 0.03 μM$^{-1}$ s$^{-1}$. *D,* the relative amplitudes of double mixing assays. 100/25 nM bovine masseter myofibrils rapidly mixed with 10/2.5 μM mant-ATP for different age times (0.2–60 s), then rapidly mixed with 250/125 μM MgATP.

stabilize the IHM state of myosin (2, 18). The binding affinity of mavacamten to BM myosin in the skinned myofibrils was examined. Figure 2A shows example transients of the BM myofibrils without and with 3 μM mavacamten, demonstrating that the slow phase becomes more prominent when mavacamten is present, with small changes in the two $k_{obs}$ values at 20 °C (Table S1). Repeating the assay with different concentrations of mavacamten at 20 °C showed that the amplitude of the slow phase had a hyperbolic dependence on mavacamten concentration (Fig. 2B), which yielded an affinity ($K_d$) of 2.1 ± 1.2 μM. The relative proportion of the slow phase increased from 26.3% to 76.2%. It should be noted that saturating mavacamten did not push all of the myosin into the SRX state. The assay was repeated for the other tissue types, namely rabbit psoas (RP) and porcine ventricle (PV: Fig. 2, *C* and *D*). The affinity of mavacamten to RP was 14.4 ± 3.2 μM and for PV was 5.2 ± 4.2 μM. The relative proportion of the slow phase

increased from 42.4% to 54.7% for the RP, while the slow phase increased from 28.4% to 90.0% for the PV. The much weaker affinity of mavacamten for fast skeletal myosin is consistent with earlier reports from purified myosin (30, 31) and myofibrils (32). Note also that the population of the SRX state was higher in RP (∼42%) than in the other two types of myofibrils (∼26% for BM; ∼28% for PV), but the increase in the SRX population induced by saturating mavacamten was much smaller for RP (max. 55%) compared with BM (76%) and PV (90%).

## Temperature effects on myofibrils without and with mavacamten

Temperature is thought to affect the proportion of myosin in the ordered thick filament with warmer temperatures encouraging the ordered structure. Using the temperature

~ASBMB

*J. Biol. Chem.* (2022) 298(3) 101640 **3**
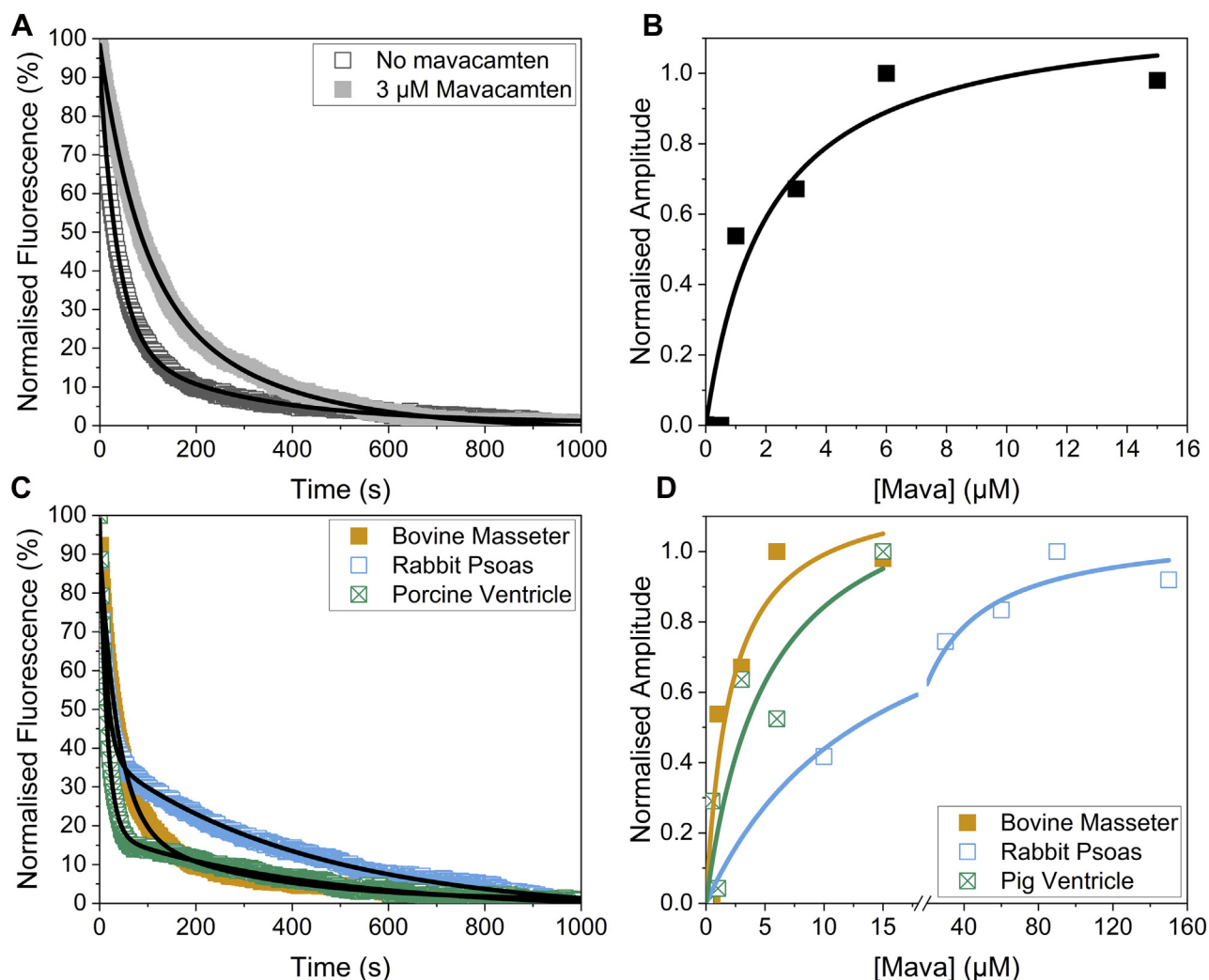
**Figure 2. Effects of mavacamten on the types of myosin heads in myofibrils.** *A,* example transients of bovine masseter myofibrils without (*open dark gray squares*) and with 3 μM mavacamten (*closed light gray squares*). These were best described by a double exponential with a fast phase $k_{obs} = 0.01252 \text{ s}^{-1}$ and a slow phase $k_{obs} = 0.00356 \text{s}^{-1}$, while the fast phase amplitude of 4.9% and a slow phase amplitude of 3.4% in the presence of mavacamten. The values for $k_{obs}$ are summarized in Table S1. *B,* mavacamten concentration dependence of the slow phase amplitude for bovine masseter myofibrils. The $K_d$ of the mavacamten for bovine masseter myofibrils was 2.1 ± 1.2 μM. *C,* example transients of bovine masseter (*orange closed squares*), rabbit psoas (*open blue squares*), and porcine ventricle (*crossed green squares*). These were both described by double exponentials with the fast phase $k_{obs} = 0.08922 \text{ s}^{-1}$ and slow phase $k_{obs} = 0.00702 \text{ s}^{-1}$ with an amplitude of 3.8% and 1.7% for the fast and slow phase respectively for the rabbit psoas myofibrils. For the porcine ventricle myofibrils, the fast phase $k_{obs} = 0.06733 \text{ s}^{-1}$ and the slow phase $k_{obs} = 0.00220 \text{ s}^{-1}$ while the amplitudes of the fast and slow phases were 5.4% and 1.3% respectively. *D,* mavacamten concentration dependence of the slow phase amplitude for bovine masseter (*closed orange squares*), rabbit psoas (*open blue squares*), and porcine ventricle (*crossed green squares*). This gave a $K_d$ of 14.4 ± 3.2 μM for rabbit psoas and 5.2 ± 4.2 μM for porcine ventricle. The values for $k_{obs}$ are summarized in Table S1.

manifold attachment to the stopped flow (developed by our lab (33)), we were able to repeat the mant-ATP displacement assays at temperatures from 5 to 30 °C (Fig. 3). For the BM (Fig. 3*A*), RP (Fig. 3*B*), and PV (Fig. 3*C*), there was little change in the % SRX state present across the temperatures studied in the absence of mavacamten. This result is in line with the report by Rohde *et al* (16), who also found little effect of temperature of the proportion of myosin in the SRX state, but in stark contrast the effect of temperature on the order to disorder transition of the thick filament. Little ordered thick filament was observed at temperature below 5 °C (13). The $k_{obs}$ values are summarized in Table S1, and the Arrhenius plots are discussed below.
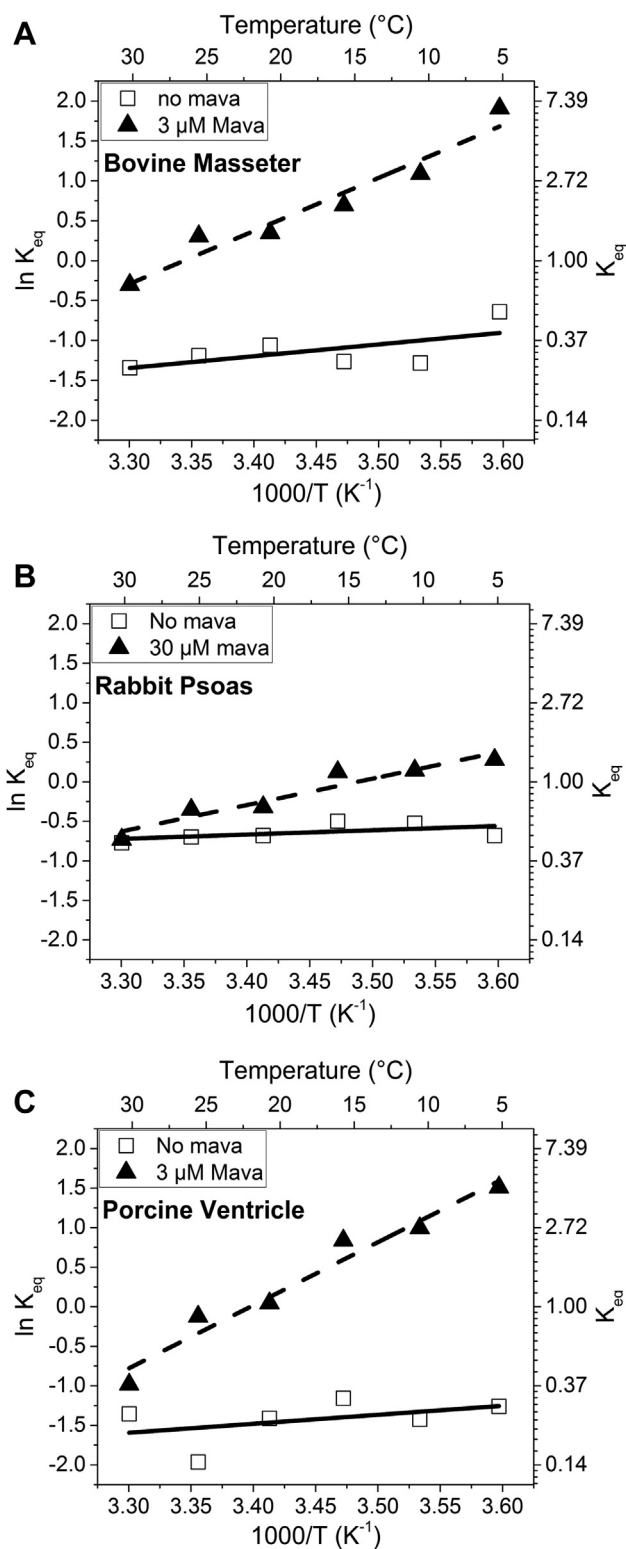
When mavacamten (at a concentration close to the $K_d$) was added to the myofibrils, the slow (SRX) phase became larger

for each muscle type (Fig. 3), but the sensitivity to mavacamten differed for each muscle type. In each case, the sensitivity to mavacamten was reduced at 30 °C compared with 5 °C (Fig. 3). At 30 °C, the amplitude of the slow (SRX) phase was similar in the presence and absence of mavacamten for both RP and PV myofibrils (Fig. 3). This is consistent with a stronger effect of mavacamten in β-myosin (dominant in the masseter and ventricle tissues) than in fast skeletal muscle myosin. However, the effect of mavacamten is reduced approaching physiological temperatures. To assess if the decreased sensitivity to mavacamten was the result of a reduced affinity, the affinity measurement of Figure 2*B* was repeated for BM myofibrils at 30 °C and showed no significant loss of mavacamten affinity. The results therefore suggest that mavacamten has a reduced ability to induce the SRX state at higher temperature.
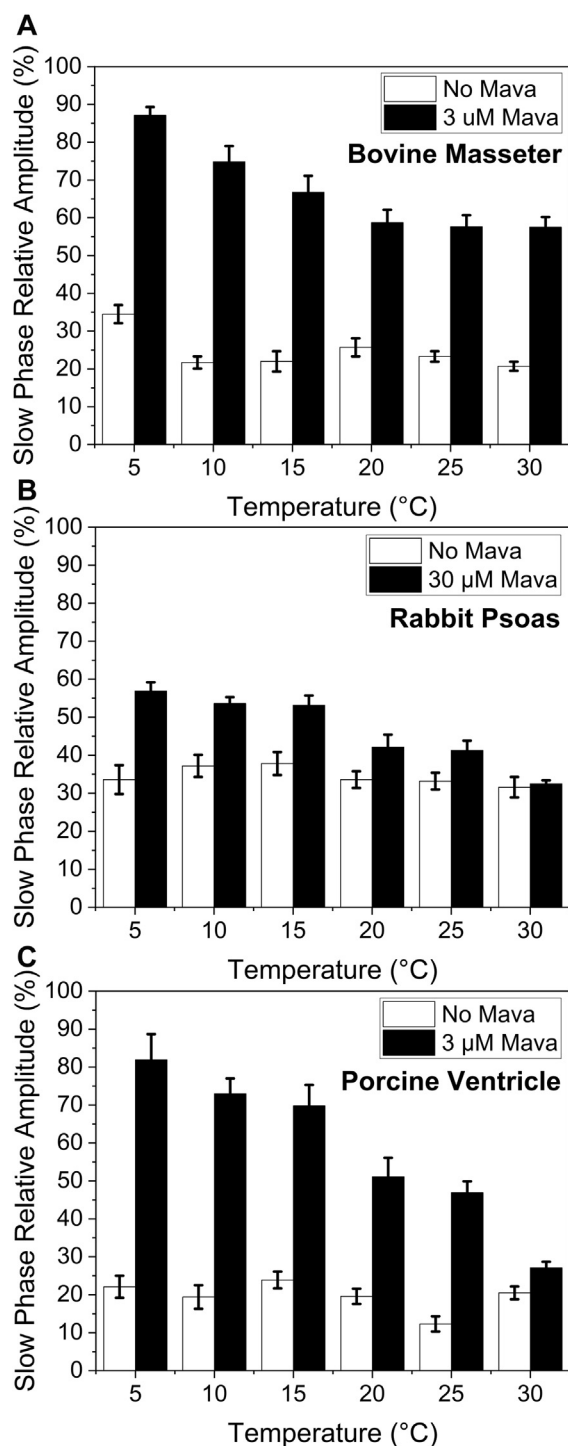
**Figure 3. Temperature dependence of relative amplitudes of the slow (SRX) phase of mantATP displacement from myofibrils.** Percentage SRX for three different muscles; bovine masseter (*A*), rabbit psoas (*B*), and porcine ventricle (*C*) in the absence (*white bars*) of and presence (*black bars*) of mavacamten. The mavacamten used was influenced by the $K_d$ determined in Figure 2. The concentration of mavacamten used was 3 μM for bovine masseter and porcine ventricle and 30 μM for rabbit psoas.



**Figure 4. Van't Hoff plot of the derived equilibrium constant between the two myosin populations for the three fiber types.** Bovine masseter (*A*), rabbit psoas (*B*), and porcine ventricle (*C*) in the absence of (*open squares*, fitted with *solid lines*) and in the presence of (*closed triangles*, fitted with *dashed lines*) mavacamten. The values are summarized in Table 1.

Assuming that the transition between SRX/IHM and active myosin heads is in equilibrium and that the ratio of fast and slow amplitudes defines the equilibrium constant ($K_{eq}$ = fast amp/slow amp), van't Hoff plots were generated over the temperature range of 5–30 °C (Fig. 4) with and without

mavacamten. The plots generated a reasonably straight line in each case with a low value of $\Delta H°$ ($<-12$ kJ mol$^{-1}$) in the absence of mavacamten, but with larger errors such that they
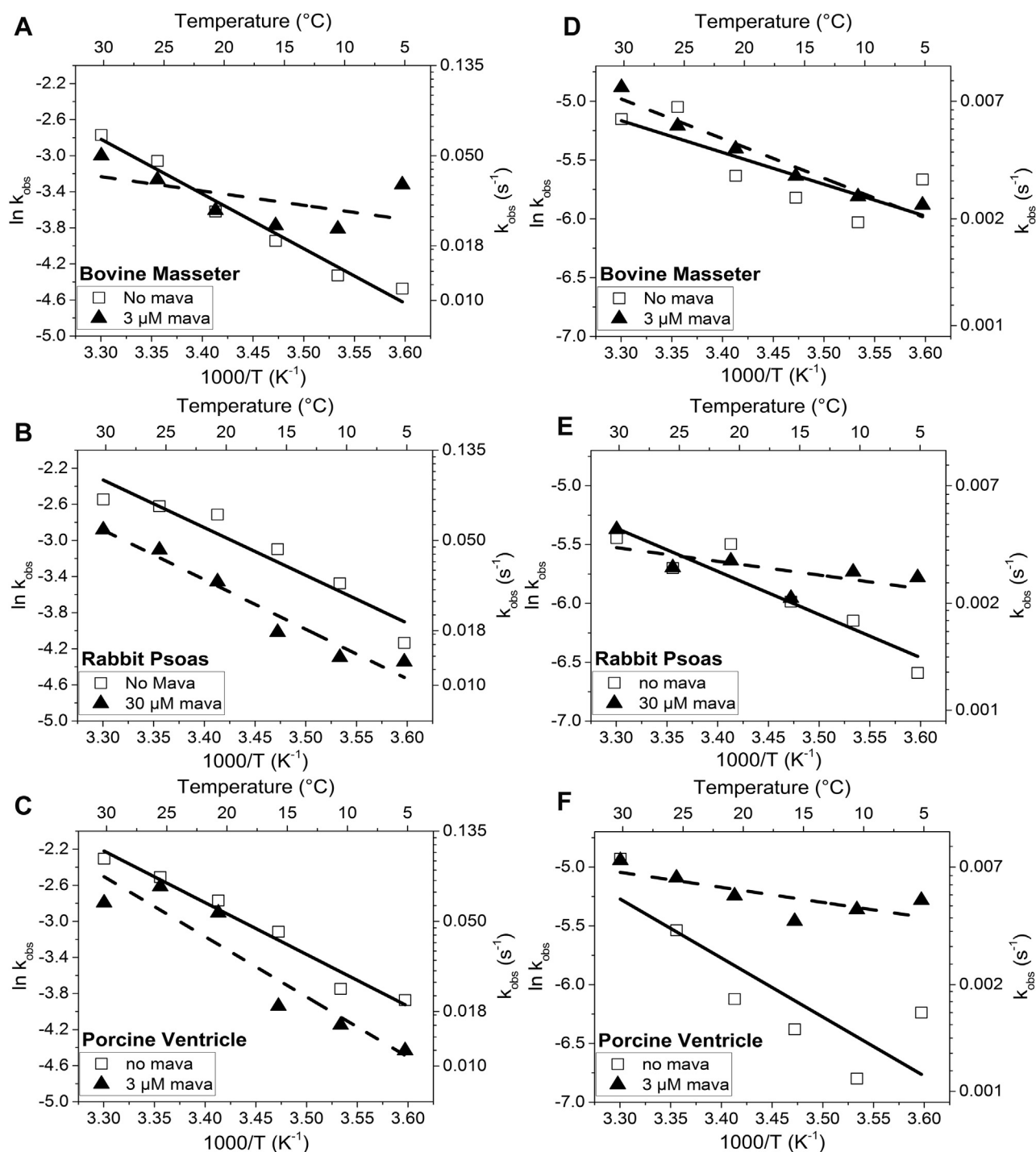
**Figure 5. Temperature dependence of $k_{obs}$ for the fast and slow phase for the three tissue types in the absence of (*open squares*, fitted with *solid lines*) and in the presence of (*closed triangles*, fitted with *dashed lines*) mavacamten.** *A–C*, Arrhenius plot of the fast phase $k_{obs}$. *D–F*, Arrhenius plot of the slow phase $k_{obs}$ from the three tissue types in the absence of (*open squares*, fitted with *solid lines*) and presence of (*open triangles*, fitted with *dashed lines*) mavacamten (3 μM for bovine masseter and porcine ventricle and 30 μM for rabbit psoas). The values for $\Delta H^{\ddagger}$ and $\Delta S^{\ddagger}$ are summarized in Table 1.

are not well distinguished from zero. In contrast, the presence of mavacamten resulted in $\Delta H^{\circ}$ values of −55, −27, and −66 kJ mol$^{-1}$ (determined from the gradient of the linear fit) for BM (Fig. 4A), RP (Fig. 4B), and PV, respectively (Fig. 4C, Table 1). The value of $K_{eq}$ at 20 °C was progressively greater for PV (0.24), BM (0.34), and RP (0.51), respectively, without mavacamten present. This compares with much higher $K_{eq}$ for

PV (1.04) and BM (1.42), but only slightly greater $K_{eq}$ for RP (0.73) in the presence of mavacamten.

The $\Delta S^{\circ}$ values (change in entropy) were also calculated from these plots (Table 1); however, the errors on values are large and therefore have little significance. On the other hand, there is an indication that $\Delta S^{0}$ decreases (a larger negative value) when mavacamten is present.

**Table 1**
Thermodynamic values from the Arrhenius and van't Hoff plots of the fast and slow phase data from Figures 4 and 5

| Myofibrils | Condition | Fast phase | | Slow phase | | Van't Hoff | |
|---|---|---|---|---|---|---|---|
| | | $\Delta H^{\ddagger}$ (kJ.mol$^{-1}$) | $\Delta S^{\ddagger}$ (J.K.mol$^{-1}$) | $\Delta H^{\ddagger}$ (kJ.mol$^{-1}$) | $\Delta S^{\ddagger}$ (J.K.mol$^{-1}$) | $\Delta H^0$ (kJ.mol$^{-1}$) | $\Delta S^0$ (J.K.mol$^{-1}$) |
| Bovine Masseter | – Mavacamten | 50.7 ± 4.2 | 143 ± 14.1 | 22.4 ± 9.1 | 31.6 ± 30.8 | −12.5 ± 7.5 | −51.5 ± 25.8 |
| | + Mavacamten | 13.3 ± 10 | 16.6 ± 34.9 | 28.3 ± 5.8 | 50.7 ± 10.0 | −54.9 ± 6.7 | −182.9 ± 24.1 |
| Rabbit Psoas | – Mavacamten | 44.1 ± 6.7 | 125.5 ± −24.1 | 30.8 ± 5.8 | 55.7 ± 20.8 | −4.2 ± 3.3 | −20.8 ± 11.6 |
| | + Mavacamten | 45.7 ± 5.0 | 126.4 ± 17.5 | 10.0 ± 5.0 | −14.1 ± 18.3 | −27.4 ± 4.2 | −97.3 ± 14.1 |
| Porcine Ventricle | – Mavacamten | 47.4 ± 4.2 | 138.8 ± 15.0 | 41.6 ± 13.3 | 93.9 ± 46.6 | −9.1 ± 9.1 | −44.1 ± 32.4 |
| | + Mavacamten | 55.7 ± 10.0 | 162.1 ± 34.9 | 10.8 ± 4.2 | −6.7 ± 15.8 | −66.5 ± 6.7 | −225.3 ± 23.3 |

$\Delta H^{\ddagger}$, change in enthalpy; $\Delta S^{\ddagger}$, change in entropy.

The Arrhenius plots for the $k_{obs}$ of fast and slow phases were also generated from the same dataset (Fig. 4) with the activation parameters $\Delta H^{\ddagger}$ and $\Delta S^{\ddagger}$ listed in Table 1. The slope of the Arrhenius plots (and hence $\Delta H^{\ddagger}$ values) for the fast phase $k_{obs}$ in the absence of mavacamten was similar for each myofibril muscle type with a >2-fold change in $k_{obs}$ across the temperature range (5–30 °C). In the presence of mavacamten, the temperature effect was markedly reduced for BM while the other two tissue types were similar.

Temperature in general had a smaller effect on the slow phase $k_{obs}$ (<2 fold) than the fast phase, but mavacamten markedly reduced the temperature sensitivity for RP and PV with little effect on BM. Thus, the effect of mavacamten on each myofibril type was opposite that seen for the fast phase. As for the van't Hoff plots, the large errors on many of the $\Delta S^{\ddagger}$ values made comparisons difficult.

### Mant-dATP effects on myofibrils

It has been shown that small amounts of 2-deoxy-ATP (dATP) in the ATP pool (1–2% of total ATP) increase the isometric force of cardiomyocytes and fractional shortening in ventricles (34–36), and this could be due to loss of the SRX. Therefore, we tested the effect of dosing mant-ATP with mant-dATP. The total concentration of mant-nucleotide was kept constant, and the percentage of mant-dATP in the mixture changed. For BM myofibrils, as the percentage of mant-dATP increased to 50%, the amplitude of the slow phase decreased approximately linearly from 30% to 18%. When 100% mant-dATP was used, the slow (SRX) phase was no longer measurable (Fig. 6A). The loss of the slow phase with 100% mant-dATP was also seen for RP (Fig. 5B) and PV (Fig. 5C); however, the concentration dependence of the mant-dATP decline in the slow phase amplitude was less pronounced than for BM in both cases.

Since mant-dATP had an opposite effect on the myofibrils to that seen with mavacamten, we investigated what would happen if 100% mant-dATP was used in relaxed myofibrils with mavacamten. Figure 5 shows how the slow phase returns when mant-dATP is added to mavacamten-treated myofibrils for all three tissue types. The biggest effect was seen in the BM myofibrils, with the slow (SRX) phase becoming larger than that seen with just mant-ATP. The other two tissues showed a smaller effect compared with the masseter, suggesting a tissue-specific effect.

### Induced-pluripotent stem cells

Human induced pluripotent stem cell–derived cardiomyocytes (hiPSC-CMs) are an emerging area of interest, and the ability to generate them using donor blood samples allows research of human myosin that is much more difficult to achieve with myectomy samples. Thus, we investigated myofibrils from 30 day postdifferentiation hiPSC-CMs. The mant-ATP chase assay was repeated with hiPSC-CM myofibrils without and with mavacamten present as well as replacing the mant-ATP with mant-dATP at 20 °C (Fig. 7). The chase experiment in the absence of mavacamten showed that the fast and slow phases were similar in population, with percentages of 58.0% and 42.0% respectively. Mavacamten had a large effect on the population of the two components by reducing the fast phase to 26.6% while increasing the slow phase to 73.4%. When mant-ATP was replaced with mant-dATP, all but one of the data points showed a loss of the slow phase. The populations of the fast and slow components were 94.0% and 6.0%, respectively. This established that the approach can be used to define the SRX state in myofibrils from hiPSC-CMs in addition to tissue samples.

### Discussion

The fluorescent ATP analog mant-ATP was first used in single turnover studies to identify the super-relaxed (SRX) state by Cooke and his associates (3, 6). This followed on from similar studies in smooth and molluscan muscle myosins (37, 38) and has since been widely used to study the SRX in single muscle fibers (39, 40), cardiomyocytes (22), isolated and synthetic myosin thick filaments as well as purified myosin and its subfragments (18). Each of these has its advantages. Here we utilized myofibrils, the small, organized muscle fragments, which consist of a few dozen sarcomeres in series and ~1 μm in diameter. The major advantage of such a preparation is that it is small enough to allow rapid diffusion of small molecules such as ATP and its fluorescent analogs through the structure, yet retains most of the features of demembranated muscle cell, including the regulatory elements of the thick filament. The myofibrils are also small and robust enough to utilize rapid mixing techniques and have been used successfully in a variety of such rapid mixing studies including stopped flow and quenched flow methods (41, 42) (for review, see (43)). A disadvantage of myofibrils is that like myosin, HMM, and myosin thick filaments, they are generally not suitable for
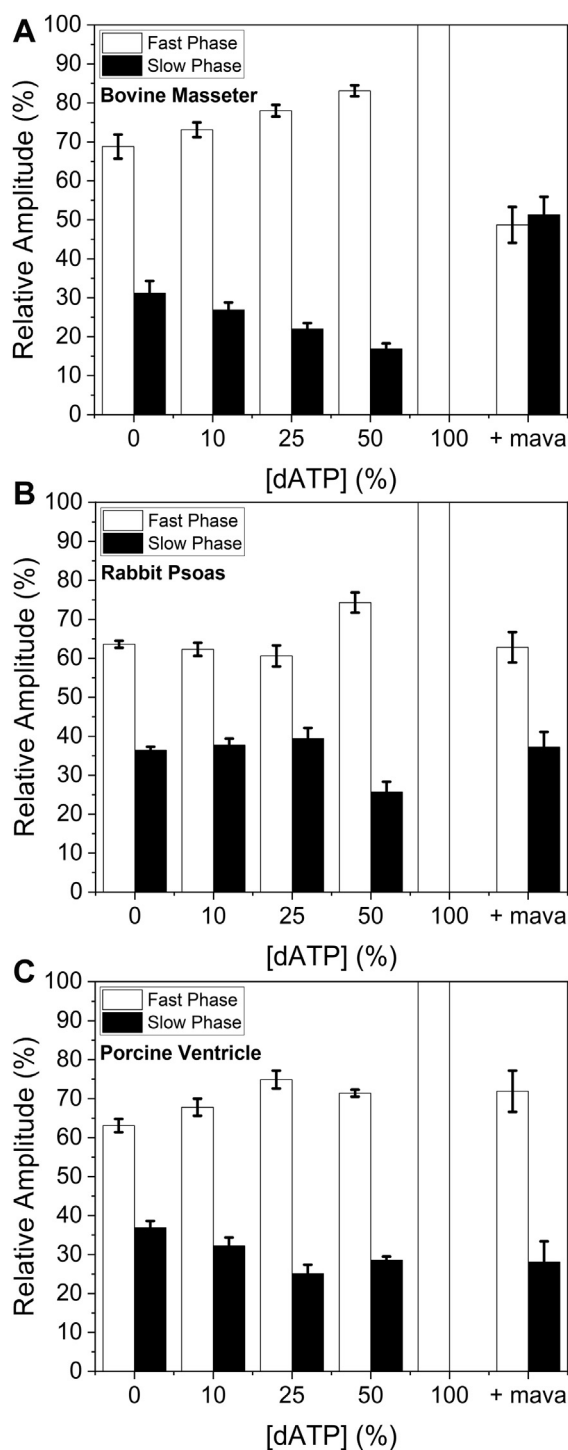
**Figure 6. Effect of mant-dATP/mant-ATP ratio on the displacement reaction for the three types of myofibrils.** Myofibrils with increasing concentrations of mant-dATP from 0 to 100%. *A*, bovine masseter myofibrils. *B*, rabbit psoas myofibrils. *C*, porcine ventricle myofibrils (fast phase in *white bars*, and slow phase in *black bars*). For each myofibril type, the data for 100% mant-dATP + mavacamten are also shown. 3 μM mavacamten for bovine masseter and porcine ventricle, 30 μM mavacamten for rabbit psoas. The values for $k_{obs}$ are summarized in Table S1.
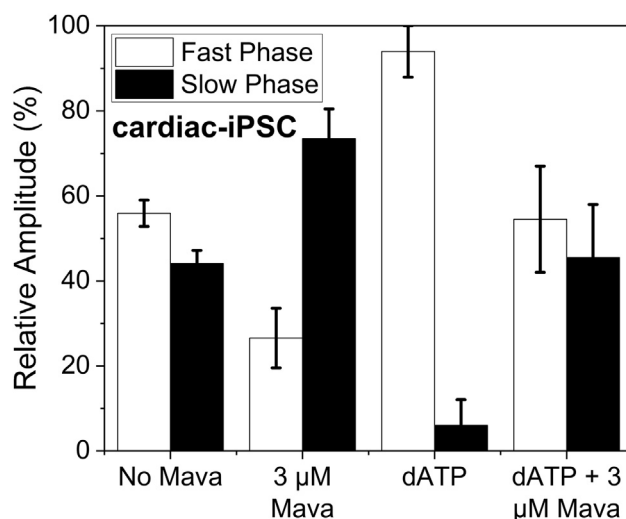


**Figure 7. Myofibrils from cardiomyocyte induced pluripotent stem cells (cm-iPSCs).** Mant-ATP dissociation assay repeated at 20 °C for stem cell myofibrils. Without mavacamten the fast (*white bars*) and slow phases (*black bars*) had an average relative population of 58.0% and 42.0%, respectively. The average fast phase $k_{obs} = 0.02749$ s$^{-1}$ and the average slow phase $k_{obs} = 0.00162$ s$^{-1}$. When mavacamten was added (3 μM), the populations changed to 26.6% and 73.4% respectively, while the average $k_{obs} = 0.03847$ s$^{-1}$ and 0.00174 s$^{-1}$ for the fast and slow phases, respectively. With mant-dATP added in place of mant-ATP, the population of fast and slow phase changed to 94.0% and 6.0% respectively with the average $k_{obs} = 0.07204$ s$^{-1}$ and 0.00142 s$^{-1}$ for the fast and slow phases, respectively. With both mant-dATP and mavacamten present, the data were similar to the control values. All amplitudes and rate constants are listed in Table S1.

affected by the concentration, average size, and degree of aggregation of the myofibrils. However, since the concentration, size, and aggregation state of myofibrils are constant in each measurement, this does not affect the measurement of the time course of the fluorescent signal change except for the first few msec after completion of the mixing. We show here that we can measure signal change of <5% even with the background scatter.

As demonstrated here (and previously (42)), sufficient quantities of myofibrils for these studies can be prepared from most muscle tissues (fast, slow, and cardiac) and from patient-derived iPSCs. In principle, the small sample size required would allow the myofibrils to be prepared from human patient biopsy samples such as those from myectomy procedures. The use of myofibrils demonstrated here could therefore be used to test for malfunction of thick filament regulation in patient samples (either biopsy or patient-derived stem cells) and to explore the potential of small-molecule drug treatments.

Here we have defined the population of myosin heads slowly turning over ATP, defined as in the SRX state. We have done this for three muscle fiber types; rabbit fast skeletal, bovine slow skeletal, and PV muscle, plus we have demonstrated the same information can be extracted from myofibrils derived from iPSCs. Each muscle has its own characteristics, but all show two populations of myosin heads that can be influenced by temperature, mavacamten, and dATP plus a combination of these treatments.

In a parallel study (N. Kad, personal communication), we also demonstrated that the same rabbit fast muscle myofibrils

systems developing force. Our studies are restricted to relaxed myofibrils.

A second disadvantage of using myofibrils is that the size of the myofibrils produces significant light scattering, which is

can be used to assess the population of myosin heads in the SRX state using single-molecule fluorescent methods. This allows the lifetime of each myosin-bound fluorescent-ATP molecule to be assessed, as well as its location within the A-band. This approach was pioneered by (44) and allows the different populations of myosin heads to be identified in the P, C, and D zones of each half A band. The total number of myosins in SRX states assessed here are compatible with numbers assessed by the single-molecule approach when averaged over the whole thick filament (≈30% SRX and 60% DRX in RP myofibrils (N. Kad, personal communication).

### Slow skeletal vs. fast skeletal muscle

The major difference between the BM and RP is the dominant myosin isoform expressed. For the BM, this is the "slow" β-myosin (>95%) (45), while for RP contains only the fast muscle myosin isoforms-2x (≈92%) and myosin-2b (≈8%) (46). When mavacamten was absent from the assay, there was ≈10% more myosin in the slow phase in the RP (34.5 ± 1%) compared with the BM (24.7 ± 2.1). The two fiber types have a very different sensitivity to mavacamten ($K_{app}$ = 2 vs 30 µM), as reported from the initial drug screening studies and also reported in myofibrils (32). In addition to the lower affinity of fast muscle fibers for mavacamten, the effect of mavacamten was also greatly reduced at all temperatures, and little or no effect was observed at physiological temperatures above 30 °C.

One major difference between the fast and slow skeletal fibers, in addition to the myosin isoforms, is the MyBP-C isoform expressed in each tissue type (47). In the relaxed muscle, MyBP-C is thought to have a role in stabilizing the SRX (21) in the thick filament C-zone, and the degree of stabilization can be modified *via* MyBP-C phosphorylation. The effects reported here could include contributions from myosin and MyBP-C isoform differences.

### Slow skeletal vs. cardiac muscle

Both BM and PV express predominantly the β-myosin isoform (45, 48) and also express different MyBP-C isoforms (47). In most respects, the SRX in the two types of myofibrils was similar, but not identical, and had a similar sensitivity to temperature, mavacamten, and dATP. Previous work using skinned PV cardiomyocytes gave a percentage SRX population of 26 ± 2% in the absence of mavacamten, with mavacamten increasing the SRX population to 39 ± 4% (2).

The simple interpretation of the data at 30 °C is that the BM and PV myofibrils have ~20% of myosins in the SRX state, a significantly smaller fraction than the RP (~32%). Therefore, the fast muscle has fewer available heads (a larger reserve) in the relaxed muscle. This situation does not change to any large extent at low temperature. In the presence of mavacamten, both BM and PV myofibrils are largely in the SRX state at 5 °C, and the effect of mavacamten reduces as temperature increases. In contrast, mavacamten not only binds approximately tenfold more weakly to RP myofibrils, but has a much smaller ability to stabilize the SRX state.

We need to consider what exactly these two populations of myosin heads described here are. In the literature, the studies of myosin and the thick filament structures have been considered in terms of an interacting head domain and order/disorder transition of the filament and the DRX/SRX state of myosin heads. These terms are not interchangeable and may not be exactly the same thing, *e.g.*, the SRX and IHD have been reported in the absence of any filament, and there are some reports of an SRX in a single-headed myosin preparation, S1 (2, 14, 16, 18). For example, is it possible to have one myosin head inhibited while the other continues to turn over ATP. Here we have defined the SRX as a myosin head (normally assumed to be a pair of heads) with a turnover rate much less than that measured for isolated single heads—*i.e.*, typically ~0.05 s⁻¹ for a single relaxed head and <0.005 s⁻¹ for an SRX head. Note, it can be difficult to distinguish a myosin head with different degrees of inhibition, *i.e.*, a myosin with a very slow or very, very slow or indeed zero turnover (considered further below). In population studies, it can also be difficult to distinguish a turned off head or inhibited myosin head from a damaged or misfolded myosin. In the latter case, the ability to change the SRX population by treatments such as mavacamten or dATP is a useful control for SRX myosin *vs.* a damaged myosin (49). It is therefore important to know if the populations observed experimentally account for the total population of myosins present. Comparing the amplitude of the fluorescence change for mant-ATP binding to a myofibril with that of the mant-ATP displacement allowed this to be confirmed.

The additional advantage of the stopped-flow technique is that the mixing is complete within a few msec, and modern equipment is stable enough to measure the signal over several hundred seconds. This is important because to gain a precise measure of the two populations in a mixture needs both phases to be well defined. Missing fast-early or slow-late parts of the signal can lead to misinterpretation of the two populations. In addition to having fast mixing, we took care to ensure each reaction had attained a stable end point, thus ensuring we had the entire reaction profile recorded.

Our study has shown that myofibrils and the stopped-flow assay can rapidly assess the SRX state for different types of myofibrils and explore the thermodynamics of the population and the effects of small molecules. However, the results show there are some difficulties with the simplest interpretation of the prevailing model of the SRX–DRX system. The two issues explored below are not unique to our data but underlie all studies of the SRX using the mant-ATP displacement approach

*Is the SRX/DRX transition of myosin heads the same as the order/disorder transition of the thick filament? Put another way, are all SRX state myosin heads ordered on the thick filament?*

The effects of temperature on the SRX state seen here in the absence of mavacamten are not those reported for the order/disorder state of the thick filament, in which low temperature favors the disordered state. They are therefore not identical. In addition, the SRX and IHD have been

ASBMB

*J. Biol. Chem.* (2022) 298(3) 101640 **9**

observed in the absence of any filament structure, *i.e.*, isolated myosin or HMM. The ordered filament can be an additional form of the SRX in which the myosin heads with without an IHD pack onto the thick filament, *i.e.*, the total SRX population includes single myosin heads in the IHD and heads packed on to the thick filament. In this case, there might be expected to be more SRX in the filament studies than for isolated myosin. In fact, the observation of myosin, in thick filaments and in HMM suggests less SRX state for thick filaments (10.55%) than for HMM (20.76% in 100 mM KCl ([18])). The opposite of what might be expected if the thick filament stabilizes the SRX form of myosin. In a recent paper, Chu *et al* (2021) ([20]) also reported a mismatch between estimates of the fraction of myosin heads in the SRX state and the IHM.

*Are the two population of myosin heads observed here in thermal equilibrium?*

The van't Hoff plots and titrations with mavacamten or dATP suggest a well-behaved equilibrium constant $K_{eq}$ = [SRX]/[DRX], *i.e.*, small amounts of thermal energy (a change in temperature) or addition of a small concentration of dATP or mavacamten can push the SRX population up or down. However, there is the problem that entry into SRX is fast ($>10$ $s^{-1}$, Fig. 1*D*), while exit appears to be very slow (0.002 $s^{-1}$). The expectation is that $K_{eq}$ = rate of entry/rate of exit or $10$ $s^{-1}$/0.002 $s^{-1}$ = 5000, *i.e.*, there should be no DRX under the standard conditions at 20 °C. How is this possible? How can these populations be readily interchangeable but have a very stable SRX at $\sim 30\%$, which turns each ATP over in several hundred seconds?

Stated another way, if the SRX is turning ATP over at 0.005 $s^{-1}$, then it cannot exit from the SRX state faster than this. To do so would allow inorganic phosphate ($P_i$) to escape from SRX *via* access to the DRX state, from which $P_i$ escape is ten times faster than from the SRX state. The extreme version of this model would be if the ATP turnover by SRX is zero, then the net rate of ATP turnover depends upon the relative value of the turnover rate for the DRX state ($k_{cat,DRX}$) and the rate of exit from SRX to DRX, $k_{exit,SRX}$

(1) If $k_{cat,DRX} >> k_{exit\ SRX}$, then net turnover the rate of exit from the SRX state, $k_{exit\ SRX}$
(2) If $k_{cat,DRX} << k_{exit\ SRX}$, then net turnover rate is $k_{cat,DRX}$ times the fraction of myosin in the DRX, = $k_{cat,DRX}$ · [DRX]/([DRX] + [SRX])

A zero turnover rate for the SRX or off-state of myosin has been proposed for molluscan muscle systems ([50]) and could be the case for the mammalian sarcomeric myosins too. A zero ATPase rate for the IHD would be consistent with the structures of the IHD where it is difficult to understand how $P_i$ could escape without destabilizing or destroying the IHD, which appears to be dependent on the M.ADP.$P_i$ conformation.

A highly cooperative thick filament transition between the order/disorder of the thick filament could potentially explain the large disparity between the apparent equilibrium constant of the DRX and SRX states and the fraction of SRX observed experimentally. Similar differences between the three regions of the thick filament (C, P, and M) could contribute to this disparity, but these factors can have no role in the SRX/DRX relationship in isolated myosin or myosin subfragments. This leaves an unsatisfactory situation where there is a wealth of experimental data defining the SRX/DRX system, but a fundamental problem remains at its core. This implies these are different types of *off state* of myosin within the SRX population, which remain to be defined.

One issue not widely discussed in using mant-ATP for this assay is that it is not identical to ATP in its interaction with myosin. Specifically the affinity of mant-ADP is for myosin much tighter than that of ADP, with a dissociation rate constant one-tenth of that of ADP ([29]). The consequences of this for the assay are that there will be more myosin.mant-ADP in the steady state than is the case for ADP. The evidence to date is that myosin-bound ADP does not form the SRX/IHD, it requires the myosin to be in the M.ADP.$P_i$ from ([6]). Thus, any myosin-bound ADP in the steady state will reduce the fraction of myosin heads in the SRX. A difference in the effect of temperature on the mant-ADP release rate constant could account for the small effect of temperature seen here. Since one effect of mavacamten is a reduction, the $P_i$ release rate constant, mavacamten could rebalance the relative rates of $P_i$ and ADP release and restore the larger effect of temperature on the SRX.

The lack of a mavacamten effect on the SRX at physiological temperature was a surprise given that this drug is now in use for some types of human hypertrophic cardiomyopathies. However, the observed lack of effect at higher temperature is correlated with reports of increased thick filament order. That is, mavacamten is more effective under conditions where thick filament order is reduced. As such, this could mean mavacamten has little effect on a normal myocyte, which has a well-ordered thick filament, but could influence myocyte with an increased level of disarray as may be the case for myocytes with many HCM-linked mutations.

Despite the underlying issues with the definition of the SRX state, which are common to all experimental studies to date, we have shown the utility of myofibrils as an experimental system to define the slowly turning over fraction (SRX) of myosin within the thick filament. The myofibril approach can potentially be used to screen small molecules to modulate the SRX state and as a diagnostic tool with patient samples derived from biopsies or iPSCs.

## Experimental procedures

### Myofibril preparation

Myofibrils were prepared from three difference tissue types: RP, BM, and PV.

Both RP and BM myofibrils were prepared as described in ([42]) with some modifications. Briefly, BM and RP muscle strips were tied to wooden sticks and equilibrated in fiber

preparation (prep) buffer, which contained: 6 mM Imidazole, 8 mM Mg-Acetate, 70 mM K-acetate, 5 mM EGTA, 7 mM ATP, 1 mM NaN$_3$, pH 7.0 (at room temperature) at 4 °C on ice. This buffer was exchanged twice before being replaced with fiber prep buffer containing 0.5% Triton X-100 and left overnight for the skinning of the muscle fibers to take place. The next day for long-term storage, the muscle fibers were equilibrated on ice for 30 min with fiber prep buffer containing 50% glycerol and kept at −20 °C.

Cardiac tissue was prepared by cutting strips of ventricle tissue ∼1 mm wide and equilibrated in fiber prep buffer. Sylgard 184 was used to pin the strips in place by pinning them to the Sylgard using pieces of tungsten wire. The strips were washed in fiber prep buffer three times at 4 °C on ice before being left overnight in fiber prep buffer containing 0.5% Triton X-100. The following day, the strips were washed twice more in prep buffer to remove the Triton X-100. A protease inhibitor cocktail tablet (cOmplete, EDTA-free protease inhibitor cocktail, Roche Diagnostics GmbH) was used in all buffers throughout. For long-term storage, the muscle fibers were then dried on tissue paper before being snap frozen and stored at −80 °C until required.

For all three tissue types, the following procedure was used. Skinned muscle fibers were dissected into smaller sections; RP could be pulled apart into smaller bundles and cut into 1–2 mm long sections while the BM and PV fibers were cut into ∼1 mm pieces. These were then placed in 1 ml myofibril stopped-flow buffer: 106 mM K-acetate, 50 mM Imidazole, 12 mM Mg-Acetate, and 2 mM EGTA, pH 7.0 in a 3 ml FPLC tube at 4 °C on ice. The sample was then homogenized (TissueRuptor II, QIAGEN) at 15,000 rpm for 10 s and slowly reduced to 0 rpm over 5 s. This was repeated once more for RP and BM and twice more for PV. The samples were then centrifuged at 2800 g in a bench top centrifuge for 10 min at 4 °C. The pellet was resuspended in 1 ml of stopped-flow buffer, and the centrifugation step repeated. The concentration of myofibrils was determined based on the A$_{280}$, using an extinction coeff 0.7 (mg/ml)$^{-1}$ cm$^{-1}$ and assuming a myosin content in the myofibril of 40%.

No live animals were used in these studies. Muscle tissue was collected in accordance with the U.K. Animals (Scientific Procedures) Act 1986 and associated guidelines.

### hiPSC-CMs

hiPSC-CMs were derived from the WTC-11 hiPSC background. The WTC11 hiPSC line (51) was generously provided by Dr Bruce Conklin (Gladstone Institute, UCSF).

Cardiomyocyte-directed differentiation was performed in a monolayer platform using a modified WNT pathway modulation protocol based off of previous reports (52, 53). Generated hiPSC-CMs were subject to 4 days of glucose starvation with 4 mM lactate supplementation to purify myocyte populations. hiPSC-CMs were harvested at 30 days postdifferentiation *via* dissociation in 0.05% trypsin and centrifuged at 1200 rpm for 5 min at room temperature. Resulting cell pellets were snap frozen until needed. At 30-day postdifferentiation, myofibrils contained a mixture of α and β myosin isoforms.

Frozen cell pellets were resuspended in 200 μl of iPSC myofibril prep buffer (6 mM Imidazole, 8 mM Mg-Acetate, 70 mM K-Acetate, 5 mM EGTA, 1 mM NaN$_3$, 5 mM EDTA, pH 7.0) and centrifuged at 2800 g for 10 min at 4 °C. Cell pellets were then suspended in iPSC myofibril fiber prep buffer containing 0.5% Triton X-100 on ice for 1 h to extract myofibrils. The resulting suspension was centrifuged at 2800 g for 10 min at 4 °C twice, replacing the buffer with 200 μl of myofibril stopped-flow buffer. The concentration of myofibrils was determined based off of the A$_{280}$ using the same method as with the tissue samples.

### Stopped-flow spectroscopy

All stopped-flow experiments were conducted on a HiTech TgK Scientific DX stopped-flow spectrometer. For investigations into different temperatures, a temperature manifold that was developed in our laboratory was used (33). This allows accurate temperature control in the range of 0–40 °C.

Stopped-flow assays were conducted with 2′/3′-O-(N-Methyl-anthanoloyl)-ATP (mant-ATP, Jena Biosciences) and 3′-O-(N-Methyl-anthraniloyl)-2′-ATP (mant-dATP, Jena Biosciences). All concentrations stated are those after mixing unless stated otherwise. Mant-ATP/mant-dATP fluorescence was excited at 365 nm and measured using a KV399 cutoff filter placed before the photomultiplier detector. For PV assays, 1 μM AP5A (concentration before mixing) was added to the myofibrils to inhibit kinases present.

This article contains supporting information.

### Data availability

All of the raw data used in this manuscript are available upon request from the corresponding author MAG (m.a. geeves@kent.ac.uk).

# The SRX state in myofibrils

## References

1. Nag, S., and Trivedi, D. V. (2021) To lie or not to lie: Super-relaxing with myosins. *Elife* **10**, 1–21

2. Anderson, R. L., Trivedi, D. V., Sarkar, S. S., Henze, M., Ma, W., Gong, H., Rogers, C. S., Gorham, J. M., Wong, F. L., Morck, M. M., Seidman, J. G., Ruppel, K. M., Irving, T. C., Cooke, R., Green, E. M., *et al.* (2018) Deciphering the super relaxed state of human β-cardiac myosin and the mode of action of mavacamten from myosin molecules to muscle fibers. *Proc. Natl. Acad. Sci. U. S. A.* **115**, E8143–E8152

3. Hooijman, P., Stewart, M. A., and Cooke, R. (2011) A new state of cardiac myosin with very slow ATP turnover: A potential cardioprotective mechanism in the heart. *Biophys. J.* **100**, 1969–1976

4. Schmid, M., and Toepfer, C. N. (2021) Cardiac myosin super relaxation (SRX): A perspective on fundamental biology, human disease and therapeutics. *Biol. Open.* **10**, bio057646

5. Toepfer, C. N., Garfinkel, A. C., Venturini, G., Wakimoto, H., Repetti, G., Alamo, L., Sharma, A., Agarwal, R., Ewoldt, J. F., Cloonan, P., Letendre, J., Lun, M., Olivotto, I., Colan, S., Ashley, E., *et al.* (2020) Myosin sequestration regulates sarcomere function, cardiomyocyte energetics, and metabolism, informing the pathogenesis of hypertrophic cardiomyopathy. *Circulation* **141**, 828–842

6. Cooke, R. (2011) The role of the myosin ATPase activity in adaptive thermogenesis by skeletal muscle. *Biophys. Rev.* **3**, 33–45

7. Liu, J., Wendt, T., Taylor, D., and Taylor, K. (2003) Refined model of the 10S conformation of smooth muscle myosin by cryo-electron microscopy 3D image reconstruction. *J. Mol. Biol.* **329**, 963–972

8. Wendt, T., Taylor, D., Trybus, K. M., and Taylor, K. (2001) Three-dimensional image reconstruction of dephosphorylated smooth muscle heavy meromyosin reveals asymmetry in the interaction between myosin heads and placement of subfragment 2. *Proc. Natl. Acad. Sci. U. S. A.* **98**, 4361–4366

9. Woodhead, J. L., Zhao, F. Q., Craig, R., Egelman, E. H., Alamo, L., and Padrón, R. (2005) Atomic model of a myosin filament in the relaxed state. *Nature* **436**, 1195–1199

10. Alamo, L., Qi, D., Wriggers, W., Pinto, A., Zhu, J., Bilbao, A., Gillilan, R. E., Hu, S., and Padrón, R. (2016) Conserved intramolecular interactions maintain myosin interacting-heads motifs explaining tarantula muscle super-relaxed state structural Basis. *J. Mol. Biol.* **428**, 1142–1164

11. Caremani, M., Brunello, E., Linari, M., Fusi, L., Irving, T. C., Gore, D., Piazzesi, G., Irving, M., Lombardi, V., and Reconditi, M. (2019) Low temperature traps myosin motors of mammalian muscle in a refractory state that prevents activation. *J. Gen. Physiol.* **151**, 1272–1286

12. Fusi, L., Huang, Z., and Irving, M. (2015) The conformation of myosin heads in relaxed skeletal muscle: Implications for myosin-based regulation. *Biophys. J.* **109**, 783–792

13. Xu, S., Offer, G., Gu, J., White, H. D., and Yu, L. C. (2003) Temperature and ligand dependence of conformation and helical order in myosin filaments. *Biochemistry* **42**, 390–401

14. Ma, W., Duno-Miranda, S., Irving, T., Craig, R., and Padrón, R. (2021) Relaxed tarantula skeletal muscle has two ATP energy-saving mechanisms. *J. Gen. Physiol.* **153**, e202012780

15. Park-Holohan, S. J., Brunello, E., Kampourakis, T., Rees, M., Irving, M., and Fusi, L. (2021) Stress-dependent activation of myosin in the heart requires thin filament activation and thick filament mechanosensing. *Proc. Natl. Acad. Sci. U. S. A.* **118**, e2023706118

16. Rohde, J. A., Roopnarine, O., Thomas, D. D., and Muretta, J. M. (2018) Mavacamten stabilizes an autoinhibited state of two-headed cardiac myosin. *Proc. Natl. Acad. Sci. U. S. A.* **115**, E7486–E7494

17. Ma, W., Childers, M., Murray, J., Moussavi-Harami, F., Gong, H., Weiss, R., Daggett, V., Irving, T., and Regnier, M. (2020) Myosin dynamics during relaxation in mouse soleus muscle and modulation by 2′-deoxy-ATP. *J. Physiol.* **598**, 5165–5182

18. Gollapudi, S. K., Yu, M., Gan, Q. F., and Nag, S. (2021) Synthetic thick filaments: A new avenue for better understanding the myosin super-relaxed state in healthy, diseased, and mavacamten-treated cardiac systems. *J. Biol. Chem.* **296**, 100114

19. Stewart, M. A., Franks-Skiba, K., Chen, S., and Cooke, R. (2010) Myosin ATP turnover rate is a mechanism involved in thermogenesis in resting skeletal muscle fibers. *Proc. Natl. Acad. Sci. U. S. A.* **107**, 430–435

20. Chu, S., Muretta, J. M., and Thomas, D. D. (2021) Direct detection of the myosin super-relaxed state and interacting-heads motif in solution. *J. Biol. Chem.* **297**, 101157

21. McNamara, J. W., Singh, R. R., and Sadayappan, S. (2019) Cardiac myosin binding protein-C phosphorylation regulates the super-relaxed state of myosin. *Proc. Natl. Acad. Sci. U. S. A.* **116**, 11731–11736

22. McNamara, J. W., Li, A., Smith, N. J., Lal, S., Graham, R. M., Kooiker, K. B., van Dijk, S. J., do Remedios, C. G., Harris, S. P., and Cooke, R. (2016) Ablation of cardiac myosin binding protein-C disrupts the super-relaxed state of myosin in murine cardiomyocytes. *J. Mol. Cell. Cardiol.* **94**, 65–71

23. Sitbon, Y. H., Diaz, F., Kazmierczak, K., Liang, J., Wangpaichitr, M., and Szczesna-Cordary, D. (2021) Cardiomyopathic mutations in essential light chain reveal mechanisms regulating the super relaxed state of myosin. *J. Gen. Physiol.* **153**, e202012801

24. Scarff, C. A., Carrington, G., Casas-Mao, D., Chalovich, J. M., Knight, P. J., Ranson, N. A., and Peckham, M. (2020) Structure of the shutdown state of myosin-2. *Nature* **588**, 515–520

25. Yang, S., Tiwari, P., Lee, K. H., Sato, O., Ikebe, M., Padrón, R., and Craig, R. (2020) Cryo-EM structure of the inhibited (10S) form of myosin II. *Nature* **588**, 521–525

26. Lee, K. H., Sulbarán, G., Yang, S., Mun, J. Y., Alamo, L., Pinto, A., Sato, O., Ikebe, M., Liu, X., Korn, E. D., Sarsoza, F., Bernstein, S. I., Padrón, R., and Craig, R. (2018) Interacting-heads motif has been conserved as a mechanism of myosin II inhibition since before the origin of animals. *Proc. Natl. Acad. Sci. U. S. A.* **115**, E1991–E2000

27. Padrón, R., Ma, W., Duno-Miranda, S., Koubassova, N., Lee, K. H., Pinto, A., Alamo, L., Bolaños, P., Tsaturyan, A., Irving, T., and Craig, R. (2020) The myosin interacting-heads motif present in live tarantula muscle explains tetanic and posttetanic phosphorylation mechanisms. *Proc. Natl. Acad. Sci. U. S. A.* **117**, 11865–11874

28. Myburgh, K. H., Franks-Skiba, K., and Cooke, R. (1995) Nucleotide turnover rate measured in fully relaxed rabbit skeletal muscle myofibrils. *J. Gen. Physiol.* **106**, 957–973

29. Woodward, S. K. A., Eccleston, J. F., and Geeves, M. A. (1991) Kinetics of the interaction of 2′(3′)-O-(N-methylanthraniloyl)-ATP with myosin subfragment 1 and actomyosin subfragment 1: Characterization of two acto-S1-ADP complexes. *Biochemistry* **30**, 422–430

30. Kawas, R. F., Anderson, R. L., Ingle, S. R. B., Song, Y., Sran, A. S., and Rodriguez, H. M. (2017) A small-molecule modulator of cardiac myosin acts on multiple stages of the myosin chemomechanical cycle. *J. Biol. Chem.* **292**, 16571–16577

31. Green, E. M., Wakimoto, H., Anderson, R. L., Evanchik, M. J., Gorham, J. M., Harrison, B. C., Henze, M., Kawas, R., Oslob, J. D., Rodriguez, H. M., Song, Y., Wan, W., Leinwand, L. A., Spudich, J. A., McDowell, R. S., *et al.* (2016) A small-molecule inhibitor of sarcomere contractility suppresses hypertrophic cardiomyopathy in mice. *Science* **351**, 617

32. Scellini, B., Piroddi, N., Dente, M., Vitale, G., Pioner, J. M., Coppini, R., Ferrantini, C., Poggesi, C., and Tesi, C. (2021) Mavacamten has a differential impact on force generation in myofibrils from rabbit psoas and human cardiac muscle. *J. Gen. Physiol.* **153**, e202012789

33. Walklate, J., and Geeves, M. A. (2015) Temperature manifold for a stopped-flow machine to allow measurements from -10 to +40 °c. *Anal. Biochem.* **476**, 11–16

34. Nowakowski, S. G., Kolwicz, S. C., Korte, F. S., Luo, Z., Robinson-Hamm, J. N., Page, J. L., Brozovich, F., Weiss, R. S., Tian, R., Murry, C. E., and

Regnier, M. (2013) Transgenic overexpression of ribonucleotide reductase improves cardiac performance. *Proc. Natl. Acad. Sci. U. S. A.* **110**, 6187–6192

35. Korte, F. S., Dai, J., Buckley, K., Feest, E. R., Adamek, N., Geeves, M. A., Murry, C. E., and Regnier, M. (2011) Upregulation of cardiomyocyte ribonucleotide reductase increases intracellular 2 deoxy-ATP, contractility, and relaxation. *J. Mol. Cell. Cardiol.* **51**, 894–901

36. Schoffstall, B., Clark, A., and Chase, P. B. (2006) Positive inotropic effects of low dATP/ATP ratios on mechanics and kinetics of porcine cardiac muscle. *Biophys. J.* **91**, 2216–2226

37. Jackson, A. P., and Bagshaw, C. R. (1988) Kinetic trapping of intermediates of the scallop heavy meromyosin adenosine triphosphatase reaction revealed by formycin nucleotides. *Biochem. J.* **251**, 527–540

38. Sellers, J. R. (1985) Mechanism of the phosphorylation-dependent regulation of smooth muscle heavy meromyosin. *J. Biol. Chem.* **260**, 15815–15819

39. Wilson, C., Naber, N., Pate, E., and Cooke, R. (2014) The myosin inhibitor blebbistatin stabilizes the super-relaxed state in skeletal muscle. *Biophys. J.* **107**, 1637–1646

40. Naber, N., Cooke, R., and Pate, E. (2011) Slow myosin ATP turnover in the super-relaxed state in tarantula muscle. *J. Mol. Biol.* **411**, 943–950

41. Ma, Y. Z., and Taylor, E. W. (1994) Kinetic mechanism of myofibril ATPase. *Biophys. J.* **66**, 1542–1553

42. Walklate, J., Ujfalusi, Z., Behrens, V., King, E. J., and Geeves, M. A. (2019) A micro-volume adaptation of a stopped-flow system; use with μg quantities of muscle proteins. *Anal. Biochem.* **581**, 113338

43. Lionne, C., Iorga, B., Candau, R., and Travers, F. (2003) Why choose myofibrils to study muscle myosin ATPase? *J. Muscle Res. Cell Motil.* **24**, 139–148

44. Nelson, S. R., Li, A., Beck-Previs, S., Kennedy, G. G., and Warshaw, D. M. (2020) Imaging ATP consumption in resting skeletal muscle: One molecule at a time. *Biophys. J.* **119**, 1050–1055

45. Toniolo, L., Maccatrozzo, L., Patruno, M., Caliaro, F., Mascarello, F., and Reggiani, C. (2005) Expression of eight distinct MHC isoforms in bovine striated muscles: Evidence for MHC-2B presence only in extraocular muscles. *J. Exp. Biol.* **208**, 4243–4253

46. Tikunov, B. A., Sweeney, H. L., and Rome, L. C. (2001) Quantitative electrophoretic analysis of myosin heavy chains in single muscle fibers. *J. Appl. Physiol.* **90**, 1927–1935

47. Yamamoto, K., and Moos, C. (1983) The C-proteins of rabbit red, white, and cardiac muscles. *J. Biol. Chem.* **258**, 8395–8401

48. Locher, M. R., Razumova, M. V., Stelzer, J. E., Norman, H. S., and Moss, R. L. (2011) Effects of low-level α-myosin heavy chain expression on contractile kinetics in porcine myocardium. *Am. J. Physiol. Heart Circ. Physiol.* **300**, H869–H878

49. Radke, M. B., Taft, M. H., Stapel, B., Hilfiker-Kleiner, D., Preller, M., and Manstein, D. J. (2014) Small molecule-mediated refolding and activation of myosin motor function. *Elife* **3**, e01603

50. Nyitrai, M., Stafford, W. F., Szent-Györgyi, A. G., and Geeves, M. A. (2003) Ionic interactions play a role in the regulatory mechanism of scallop heavy meromyosin. *Biophys. J.* **85**, 1053

51. Kreitzer, F. R., Salomonis, N., Sheehan, A., Huang, M., Park, J. S., Spindler, M. J., Lizarraga, P., Weiss, W. A., So, P. L., and Conklin, B. R. (2013) A robust method to derive functional neural crest cells from human pluripotent stem cells. *Am. J. Stem Cells* **2**, 119–131

52. Lian, X., Hsiao, C., Wilson, G., Zhu, K., Hazeltine, L. B., Azarin, S. M., Raval, K. K., Zhang, J., Kamp, T. J., and Palecek, S. P. (2012) Robust cardiomyocyte differentiation from human pluripotent stem cells via temporal modulation of canonical Wnt signaling. *Proc. Natl. Acad. Sci. U. S. A.* **109**, E1848–E1857

53. Palpant, N. J., Pabon, L., Roberts, M., Hadland, B., Jones, D., Jones, C., Moon, R. T., Ruzzo, W. L., Bernstein, I., Zheng, Y., and Murry, C. E. (2015) Inhibition of β-catenin signaling respecifies anterior-like endothelium into beating human cardiomyocytes. *Development* **142**, 3198–3209